Proceedings of the EuroGNC 2013, 2nd CEAS Specialist Conference
on Guidance, Navigation & Control, Delft University of Technology,
Delft, The Netherlands, April 10-12, 2013

A New Joint Sensor Based Backstepping Control Approach for Fault-Tolerant Flight Control

L. G. Sun and Q. P. Chu and C. C. de Visser

Abstract Recently, an incremental type sensor based backstepping (SBB) control law, based on singular perturbation theory, was proposed. This Lyapunov function based method uses measurement data rather than the model knowledge, and has the advantage that the model uncertainty plays only a minor role. In this paper, the above mentioned SBB method has been extended to deal with fault tolerant flight control when failures occur to the aircraft. A new double-loop joint SBB attitude controller, as well as a hybrid nonlinear dynamic inversion (NDI)/SBB attitude controller, has been developed for a Boeing 747-200 aircraft. The benchmarks namely rudder runaway case and engine separation scenario are employed to evaluate the proposed methods. The simulation results show that the proposed joint SBB attitude control method can achieve a zero-error tracking performance in nominal condition and can guarantee the stability of the closed-loop system, under the aforementioned two failures, as long as the reference commands are achievable. Comparing with the hybrid NDI/SBB method, the joint SBB attitude control setup has an advantage in eliminating the tracking error of the sideslip angle without needing the onboard model information.

1 Introduction

Study on previous flight accidents [14] and the corresponding fault-tolerant flight control (FTFC) strategies suggests that, under many post-failure circumstances, a

L. G. Sun
Delft University of Technology, Delft, The Netherlands, 2600GB, e-mail: L.sun@tudelft.nl

Q.P. Chu
Delft University of Technology, Delft, The Netherlands, 2600GB e-mail: q.p.chu@tudelft.nl

C. C. de Visser
Delft University of Technology, Delft, The Netherlands, 2600GB e-mail: c.c.devisser@tudelft.nl

certain level of flight performance is still achievable for the aircraft with the remaining and valid control effectors, even though the control authority or the safe flight envelope have already been slightly or greatly cut down due to the structure/actuator failures.

Achievements by the Flight Mechanics Action Group 16 (FM-AG16), a branch of the Group for Aeronautical Research and Technology in Europe (GARTEUR), indicate that the 'loss of control in flight' type of accidents, which count for as much as 17% of all aircraft accidents [1], can be avoided by taking suitable control strategies[14], like for example fault detection and isolation (FDI), and reconfigurable control [9] based on online aerodynamic model identification. The El Al flight 1862 and rudder runaway scenarios, together with the other four fault scenarios, have been embedded into the Reconfigurable Control for Vehicle Emergency Relief (RECOVER) benchmark model by the FM-AG 16 group aiming at providing an assessment platform for modern fault detection and isolation (FDI) methods, and fault tolerant control (FTC) strategies[14]. With respect to propulsion control, a propusion-controlled aircraft (PCA) system has been developed in NASA Dryden Research Center, and first evaluated on a piloted B-720 simulation [6]. Subsequently, further research on PCA system has also been carried out by NASA Dryden and Ames Research Centers[16], like for example the simulations and actual flight tests of diferent flight platforms. In the PCA system, differential thrust was used as an emergency substitute for failed control surfaces[3], such as vertical tail loss with no rudder authority or the above mentioned rudder runaway case[16, 5].

Suggested by the literature Smaili et al. [14], Alwi and Edwards et al.[2] and Lombaerts and Smaili et al.[10], a powerful and advanced control approach is very essential to increase the operational performance of the post-failure aircraft. It is necessary for the chosen control algorithms to enjoy a few merits. The control methods should be robust to the sudden structural changes of the aircraft, or they should not require an accurate and full aerodynamic model, or they contain a powerful model identification module to provide the required accurate model information for the FDI and FTC units in real-time.

A number of new FTFC methods have been proposed in the literature [11, 17, 18, 2]. More recently, the work in Lombaerts et al. [10], as a part of the GARTEUR FM-AG 16 program, provided practical validation results of an piloted adaptive nonlinear dynamic inversion (ANDI) controller, the kernel of which is a two-step online physical model identification approach, on the Simulation, Motion, and Navigation (SIMONA) research simulator (SRS). In this work, the rudder runaway case, the El Al flight 1862 fault and the stabilizer runaway scenario were intensively studied, and promising results, in terms of stabilizing the post-failure aircraft or safely landing the aircraft, were obtained. Thereafter, Alwi and Edwards et al.[2] carried out another series of validation experiments on the SRS, whereas the reconfigurable controller was designed using a model reference sliding mode control method together with a fixed control allocation approach. In this work, only the El Al flight 1862 scenario was evaluated on the SRS platform. The sliding mode based control method, which is featured for not relying on the information of the failure and the extent of the damage to the airframe, has proven to be able to guarantee the stabil-

ity of the closed-loop system subject to a certain class of model uncertainties and structural/actuator changes caused by the right engine separation.

In 2007, Hovakimyan et al.[8] proposed an advanced controller for non-affine systems, which involves the singular perturbation theory, Tikhonov's Theorem and a backstepping strategy. Thereafter, Falkena and van Oort et al. [4] investigated the SBB method in further and extended its application. The control performance of SBB method was evaluated on a system with uncertainties after being utilized to design a controller for the aircraft moment equations. Indicated by the literature [8, 4], as a result of the backstepping control technique, the system stability can be guaranteed by using Lyapunov functions in this SBB approach. In addition, similar to the incremental NDI flight control scheme, the need for adaptation to uncertain parameters or unknown model structure, which is essential to most model-based conventional backstepping or adaptive NDI control approaches, is circumvented by using measurements of state derivatives rather than the full knowledge of the model, which is subject to any changes.

The objective of this paper is to present an alternative to the current FTFC methods. A new incremental type of sensor based backstepping (SBB) approach, which is insensitive to and competent to cope with the aerodynamic model changes induced by the failure scenarios, is developed and evaluated. This paper uses a similar SBB controller as that presented in [4], but the focus of this paper is on extending its application and designing an angular hold/change controller for a large civil aircraft for FTFC purpose. In this paper, an overall SBB controller for both attitude loop and body angular rate loop are designed. For comparison purpose, another hybrid attitude hold/change controller, where the outer loop uses NDI control method, is also designed. The El Al flight 1862 scenario and the rudder runaway scenario, which are two of the most challenging failure scenarios embedded in the RECOVER benchmark model, are utilized to validate the new SBB control methods.

Section 2 introduces the RECOVER benchmark model. The basic aircraft motion equations and the ANDI control method are provided in section 3. Thereafter, the single-loop body angular rate controller based on sensor based backstepping (SBB) approach, as well as a hybrid NDI/SBB attitude controller, is presented in section 4. Section 5 focuses on presenting the joint SBB attitude controller. Section 6 presents the simulation results and the corresponding analysis. Finally, concluding remarks are given.

2 Validation Platform

The El Al flight 1862 scenario and the rudder runaway fault case, embedded in the RECOVER benchmark model, are employed to validate the new control methods proposed in this paper. The RECOVER benchmark model has been discussed in detail in [15] [13]. As the kernel of the benchmark model, a mathematic model of Boeing 747-100/200 with high fidelity is used. In terms of aircraft simulation in post-failure situation, six failed scenarios are embedded.

2.1 Rudder Runaway and Engine Separation Scenarios

In this paper, only the rudder runaway and engine separation failure scenarios are utilized to validate the new sensor based backstepping methods. As indicated by [10], the rudder runaway, as well as the engine separation failure, is one of the most challenging failure in terms of recovering the aircraft into a safe flight envelope.

The losses and the remaining functional control surfaces in El Al flight 1862 are summarized as follows.

1. Lost surfaces due to the loss of hydraulic systems: outboard trailing-edge flaps, δ_{aor}, δ_{sp1}
   $\delta_{sp4-5}, \delta_{sp8-9}, \delta_{sp12}, \delta_{eil}$, δ_{eor}.
2. Functional but affected surfaces: horizontal stabilizer (half trim rate), $\delta_{air}, \delta_{ail}$ (both at half rate), and the lower rudder δ_{rl} (lag).
3. Fully functional surfaces: inboard trailing-edge flaps, δ_{sp2-3}, the left outboard elevator δ_{eol}, and the right inboard elevator δ_{eir}.

In the rudder runaway case, the rudder deflects to the left, inducing a yawing tendency of the aircraft to the left. Since the aerodynamic blow-down is taken into account in the RECOVER simulation model, the rudder deflection limit is this scenario depends on the flight speed. As a result, the maximum rudder deflection is slightly below 15 *deg* for an airspeed around 270 *kt* and even close to 25 *deg* for an airspeed approaching 165 *kt*.

For the rudder runaway case, the configuration of the attitude change/hold controller using both NDI and SBB control methods is plotted in Fig. 1(a), where $\mathbf{u} = [\delta_a, \delta_e, \triangle P_e]$ with P_e the engine pressure ratio (EPR). For the engine separation failure, the configuration of the attitude change/hold controller using differential thrusts is given in Fig. 1(b), where $\mathbf{u} = [\delta_a, \delta_e, \delta_r]$.

In both control block diagrams, the control variables are $\mathbf{w} = [p, q, r]$ in the inner loop and $[\phi, \theta, \beta]$ in the outer loop.

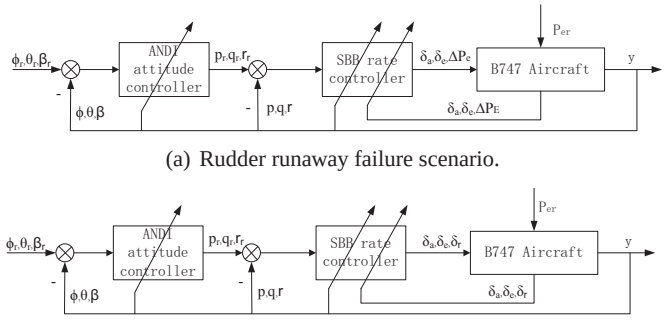

(a) Rudder runaway failure scenario.

(b) Engine separation failure scenario.

Fig. 1 Fault-tolerant controller configuration.

3 Baseline Attitude Controller using ANDI

3.1 Attitude hold controller

According to the ANDI control method, the desired commands for the inner loop are derived from the angular control loop as follows:

$$\begin{bmatrix} p_c \\ q_c \\ r_c \end{bmatrix} = \begin{bmatrix} 1 & \sin\phi\tan\theta & \cos\phi\tan\theta \\ 0 & \cos\phi & -\sin\phi \\ \frac{w}{\sqrt{u^2+w^2}} & 0 & \frac{-u}{\sqrt{u^2+w^2}} \end{bmatrix}^{-1} \left(\begin{bmatrix} \nu_\phi \\ \nu_\theta \\ \nu_\beta \end{bmatrix} - \begin{bmatrix} 0 \\ 0 \\ A_\beta \end{bmatrix} \right) \tag{1}$$

with

$$A_\beta = \frac{1}{\sqrt{u^2+w^2}} \left[\frac{-uv}{V^2} \left(A_x - g\sin\theta\right) + \left(1 - \frac{v}{V^2}\right) \left(A_y + g\sin\phi\cos\theta\right) - \frac{vw}{V^2} \left(A_z + g\cos\phi\cos\theta\right) \right] \tag{2}$$

where A_x, A_y, A_z are the acceleration in the body reference frame without the gravitational effects, and $\left[\nu_\phi \ , \nu_\theta \ , \nu_\beta \right]^\top$ is the virtual angular command vector.

3.2 Rate Control and Control Allocation (CA)

As presented in [9], the control inputs can be retreated using the following formulations:

$$\mathbf{M}_{CA} \cdot \mathbf{u} = \left\{ \frac{\mathbf{I}}{\frac{1}{2}\rho V^2 S} \left(\begin{bmatrix} v_p \\ v_q \\ v_r \end{bmatrix} + \mathbf{I}^{-1} \begin{bmatrix} p \\ q \\ r \end{bmatrix} \times \left(\mathbf{I} \begin{bmatrix} p \\ q \\ r \end{bmatrix} \right) \right) - \begin{bmatrix} bC_{l_{states}} \\ \bar{c}C_{m_{states}} \\ bC_{n_{states}} \end{bmatrix} \right\} \tag{3}$$

with

$$\mathbf{M}_{CA} = \begin{bmatrix} b & 0 & 0 \\ 0 & \bar{c} & 0 \\ 0 & 0 & b \end{bmatrix} \mathbf{M}_E \tag{4}$$

where $\mathbf{M}_{CA}$ is the control allocation matrix, $\mathbf{M}_E$ is the control effectiveness matrix, $\mathbf{u}$ is the vector containing all the control inputs and $C_{l_{states}}, C_{m_{states}}, C_{n_{states}}$ are the nondimensional moments contributed by all of the current states. For aerodynamic model identification to get the above mentioned unknown parameters such as $\mathbf{M}_E$, the two-step estimation method from [9] has proven to be an effective method. The Boeing 747-200 aircraft has 30 independent control inputs including 25 deflectable control surfaces, 4 engine pressure ratios (EPRs) and 1 flight gear control input, see the literature [14]. However, for simplification purpose, some of them can still be emerged to get the following 19 equivalent and active control variables as suggested by Alwi and Edwards et al.[2][7], and Vahram et al. [16].

$$\mathbf{u} = \left[\delta_a, \delta_{sp}, \delta_e, \delta_{ih}, \delta_r, P_e, \triangle P_e\right]^\top \tag{5}$$

with

$$\begin{aligned}
\delta_a &= [\delta_{air}, \delta_{ail}, \delta_{aor}, \delta_{aol}] \\
\delta_{sp} &= [(\delta_{sp1} + \delta_{sp4}), (\delta_{sp2} + \delta_{sp3}), (\delta_{sp10} + \delta_{sp11}), (\delta_{sp9} + \delta_{sp12})] \\
\delta_e &= [\delta_{eir}, \delta_{eil}, \delta_{eor}, \delta_{eol}] \\
\delta_r &= [\delta_{ru}, \delta_{rl}] \\
P_e &= \left[P_{e_1}, P_{e_2}, P_{e_3}, P_{e_4}\right] \\
\triangle P_e &= \frac{1}{4}\left[(P_{e_1} - P_{e_4}) + \left(P_{e_2} - P_{e_3}\right)\right]
\end{aligned} \tag{6}$$

In the process of online aerodynamic model identification, we can select 19 regressors for C_X :

$$[1, \alpha, \alpha^2, \frac{q\bar{c}}{V}, \delta_{sp}, \delta_e, \delta_{ih}, \delta_{flap_1}, \delta_{flap_2}, P_e]$$

18 regressors are selected for C_Z and C_M:

$$[1, \alpha, \frac{q\bar{c}}{V}, \delta_{sp}, \delta_e, \delta_{ih}, \delta_{flap_1}, \delta_{flap_2}, P_e]$$

15 regressors are selected for C_Y C_L and C_N:

$$[1, \beta, \frac{pb}{2V}, \frac{rb}{2V}, \delta_a, \delta_{sp}, \delta_r, \triangle P_e]$$

The matrix $\mathbf{M}_E$ shown in Eq. 3 can have as many as 19 columns at most according to Eq. 5, and a dynamic quadratic programming (DQP) based CA method from [7] has proven to be a powerful approach to calculate the control inputs $\mathbf{u}$ in Eq. 3. However, in order to show merely the high performance of the new control methods proposed in this paper, the $\mathbf{M}_E$ matrix is selected to have the following simplified form for later usage in this paper:

$$\mathbf{M}_E = \begin{bmatrix} \tilde{C}_{l\delta_a} & 0 & \tilde{C}_{l\delta_r} \\ 0 & \tilde{C}_{m\delta_e} & 0 \\ \tilde{C}_{n\delta_a} & 0 & \tilde{C}_{n\delta_r} \end{bmatrix} \tag{7}$$

with

$$\begin{aligned}
\tilde{C}_{l\delta_a} &= -C_{l\delta_{air}} + C_{l\delta_{ail}} - C_{l\delta_{aor}} + C_{l\delta_{aol}} - \\
&\quad C_{l\delta_{sp1}} - \cdots - C_{l\delta_{sp4}} + C_{l\delta_{sp9}} + \cdots + C_{l\delta_{sp12}} \\
\tilde{C}_{n\delta_a} &= -C_{n\delta_{air}} + C_{n\delta_{ail}} - C_{n\delta_{aor}} + C_{n\delta_{aol}} - \\
&\quad C_{n\delta_{sp1}} - \cdots - C_{n\delta_{sp4}} + C_{n\delta_{sp9}} + \cdots + C_{n\delta_{sp12}} \\
\tilde{C}_{m\delta_e} &= C_{m\delta_{eir}} + C_{m\delta_{eil}} + C_{m\delta_{eor}} + C_{m\delta_{eol}} \\
\tilde{C}_{l\delta_r} &= C_{l\delta_{ru}} + C_{l\delta_{rl}} \\
\tilde{C}_{n\delta_r} &= C_{n\delta_{ru}} + C_{n\delta_{rl}}
\end{aligned} \tag{8}$$

Note that, Eq. 8 also implies that the control surfaces that belongs to the same category will get equal deflecting commands. In addition, the following relationship exists:

$$\begin{aligned} P_{e_1} &= P_{e_2} = mean\,(P_{e_r}) + \triangle P_e \\ P_{e_3} &= P_{e_4} = mean\,(P_{e_r}) - \triangle P_e \end{aligned} \tag{9}$$

4 Hybrid NDI/SBB Attitude Controller

A new hybrid NDI/SBB attitude controller is designed for the Boeing 747-200 model embedded in the RECOVER benchmark model. In the outer loop, the NDI control method as shown in Eq. 1 is utilized to design an attitude controller. While, the SBB control approach is employed to design the body angular rate controller in the inner loop.

4.1 Perturbation Theory based Incremental Backstepping

The singular perturbation theory (SPT) based nonlinear control method was firstly presented by Slotine et al.[12], and then was widely investigated by Hovakimyan et al.[8], Falkena et al.[4]. By combining the time-scale separation property, which is the prerequisite of applying singular perturbation theory, with backstepping approach, the SBB control method presented in [8] can both guarantee the stability of the closed-loop system and avoid the requirement of accurate aerodynamic model knowledge[4].

The following expression holds for the body angular rate aerodynamics:

$$\begin{bmatrix} \dot{p} \\ \dot{q} \\ \dot{r} \end{bmatrix} = -\left\{ \left(\begin{bmatrix} p \\ q \\ r \end{bmatrix} \times \left(\mathbf{I} \begin{bmatrix} p \\ q \\ r \end{bmatrix} \right) \right) - \frac{1}{2}\rho V^2 S \cdot \mathbf{I}^{-1} \begin{bmatrix} bC_{l_{states}} \\ \bar{c}C_{m_{states}} \\ bC_{n_{states}} \end{bmatrix} \right\} + \frac{1}{2}\rho V^2 S \cdot \mathbf{I}^{-1} M_{CA} \cdot \mathbf{u} \tag{10}$$

A single-loop backstepping controller is designed as follows:

$$\begin{aligned} \mathbf{x} = \mathbf{w} &= \left[\, p\,, q\,, r \,\right]^\top \\ \mathbf{e} &= \mathbf{x} - \mathbf{y}_r \\ V\,(e) &= \frac{1}{2}\mathbf{e}^2 + \frac{1}{2}k_1\lambda^2 \\ \dot{V}\,(\mathbf{e}) &= \mathbf{e}\dot{\mathbf{e}} + k_1\lambda\,\mathbf{e} \end{aligned} \tag{11}$$

The desired system can be selected as:

$$\dot{\mathbf{e}} = -\mathbf{c}\,(\mathbf{x} - \mathbf{y}_r) \tag{12}$$

with $\mathbf{c} > 0$ to stabilize the system. Note that an integral term $\lambda = \int_0^t \mathbf{e} dt$ is introduced in order to remove the tracking errors caused by the internal dynamics. In combination with Eq. 11, we can get:

$$\mathbf{x}_{des} = \mathbf{e} + \mathbf{y}_r \tag{13}$$

$$\dot{\mathbf{x}}_{des} = \dot{\mathbf{e}} + \dot{\mathbf{y}}_r \tag{14}$$

Using Eq. 12, we get

$$\begin{aligned} \dot{V}(\mathbf{e}) &= \mathbf{e}\dot{\mathbf{e}} + k_1\lambda\mathbf{e} = \mathbf{e}(\dot{\mathbf{x}}_{des} - \dot{\mathbf{y}}_r + \mathbf{k}_1\lambda) \\ \dot{\mathbf{x}}_{des} &= -\mathbf{c}(\mathbf{x} - \mathbf{y}_r) + \dot{\mathbf{y}}_r - \mathbf{k}_1\lambda \end{aligned} \tag{15}$$

We will use the following notation later:

$$\mathbf{u}_{red} = \mathbf{M}_{CA} \cdot \mathbf{u} \tag{16}$$

with $\mathbf{u}_{red}$ a three dimensional vector denoting the equivalent inputs. According to [8], the SBB controller takes the following form:

$$\begin{aligned} \varepsilon\dot{\mathbf{u}}_{red} &= -sgn\left(\frac{\partial\dot{\mathbf{x}}}{\partial\mathbf{u}_{red}}\right)[\dot{\mathbf{x}} - \dot{\mathbf{x}}_{des}] \\ &= -sgn\left(\frac{\partial\dot{\mathbf{x}}}{\partial\mathbf{u}_{red}}\right)[\dot{\mathbf{x}} + \mathbf{c}(\mathbf{x} - \mathbf{y}_r) - \dot{\mathbf{y}}_r + \mathbf{k}_1\lambda] \end{aligned} \tag{17}$$

From Eq. 10, we get:

$$-sgn\left(\frac{\partial\dot{\mathbf{x}}}{\partial\mathbf{u}_{red}}\right) = -sgn\left(\frac{1}{2}\rho V^2 S \cdot \mathbf{I}^{-1}\right) \tag{18}$$

Thus, the controller can be designed as follows:

$$\dot{\mathbf{u}}_{red} = -sgn\left(\frac{1}{2\cdot\varepsilon}\rho V^2 S \cdot \mathbf{I}^{-1}\right)[\dot{\mathbf{x}} + \mathbf{c}(\mathbf{x} - \mathbf{y}_r) - \dot{\mathbf{y}}_r + \mathbf{k}_1\lambda] \tag{19}$$

where we select $\varepsilon = 0.1$, therefore $\mathbf{u}_{red}$ can be calculated. According to Eq. 16, we have

$$\dot{\mathbf{u}}_{red} = \mathbf{M}_{CA} \cdot \dot{\mathbf{u}} \tag{20}$$

where we assumed that $\mathbf{M}_{CA}$ is changing extremely slowly. Thus, $\dot{\mathbf{u}}$ can be calculated from Eq. 20 using a control allocation algorithm:

$$\mathbf{u}_k = \mathbf{u}_{k-1} + \int_{(k-1)T}^{kT} \dot{\mathbf{u}} \cdot dt \tag{21}$$

Note that, if $\mathbf{M}_{CA}$ is not available but $\mathbf{u}$ is of 3 dimensional, then the term $\frac{\partial\dot{\mathbf{x}}}{\partial\mathbf{u}_{red}}$ in Eq. 17 and Eq. 18 can be directly substituted by $\frac{\partial\dot{\mathbf{x}}}{\partial\mathbf{u}}$, and Eq. 18 becomes:

$$-sgn\left(\frac{\partial\dot{\mathbf{x}}}{\partial\mathbf{u}_{red}}\right) = -sgn\left(\frac{1}{2}\rho V^2 S \cdot \mathbf{I}^{-1}\mathbf{M}_{CA}\right) \tag{22}$$

Only the sign of the diagonal elements in the right hand side matrix are needed by the controller.

5 Joint Attitude/Angular Rate Controller using SBB Approach

In order to fully explore the potential advantage of the backstepping based control method in designing a multi-loop controller, like for example eliminating the tracking error of the sideslip angle even when the aircraft has been damaged to some degree, a joint attitude angle and angular rate controller with two backstepping control loops is developed.

Combining the angular motion equations with Eq. 10, we get the aerodynamic equations of the Boeing 747-200 aircraft with the following expression:

$$\begin{aligned}
\begin{bmatrix} \dot{\phi} \\ \dot{\theta} \\ \dot{\beta} \end{bmatrix} &= \begin{bmatrix} 1 & \sin\phi\tan\theta & \cos\phi\tan\theta \\ 0 & \cos\phi & -\sin\phi \\ \frac{w}{\sqrt{u^2+w^2}} & 0 & \frac{-u}{\sqrt{u^2+w^2}} \end{bmatrix} \begin{bmatrix} p \\ q \\ r \end{bmatrix} + \begin{bmatrix} 0 \\ 0 \\ A_\beta \end{bmatrix} \\
\begin{bmatrix} \dot{p} \\ \dot{q} \\ \dot{r} \end{bmatrix} &= -\left\{ \left(\begin{bmatrix} p \\ q \\ r \end{bmatrix} \times \left(\mathbf{I} \begin{bmatrix} p \\ q \\ r \end{bmatrix} \right) \right) - \frac{1}{2}\rho V^2 S \cdot \mathbf{I}^{-1} \begin{bmatrix} bC_{l_{states}} \\ \bar{c}C_{m_{states}} \\ bC_{n_{states}} \end{bmatrix} \right\} + \frac{1}{2}\rho V^2 S \cdot \mathbf{I}^{-1} M_{CA} \cdot \mathbf{u}
\end{aligned} \tag{23}$$

For later control designing usage, we let

$$\begin{aligned}
\mathbf{x}_1 &= \begin{bmatrix} \phi & \theta & \beta \end{bmatrix}^\top \\
\mathbf{x}_2 &= \begin{bmatrix} p & q & r \end{bmatrix}^\top \\
\mathbf{y}_r &= \begin{bmatrix} \phi_r & \theta_r & \beta_r \end{bmatrix}^\top \\
\mathbf{f}(\mathbf{x}_1) &= \begin{bmatrix} 0 & 0 & A_\beta \end{bmatrix}^\top \\
\mathbf{g} &= \begin{bmatrix} 1 & \sin\phi\tan\theta & \cos\phi\tan\theta \\ 0 & \cos\phi & -\sin\phi \\ \frac{w}{\sqrt{u^2+w^2}} & 0 & \frac{-u}{\sqrt{u^2+w^2}} \end{bmatrix} \\
\mathbf{k} &= \frac{1}{2}\rho V^2 S \cdot \mathbf{I}^{-1} \mathbf{M}_{CA} \\
\mathbf{h}(\mathbf{x}_2) &= -\left(\begin{bmatrix} p \\ q \\ r \end{bmatrix} \times \left(\mathbf{I} \begin{bmatrix} p \\ q \\ r \end{bmatrix} \right) \right) + \frac{1}{2}\rho V^2 S \cdot \mathbf{I}^{-1} \begin{bmatrix} bC_{l_{states}} \\ \bar{c}C_{m_{states}} \\ bC_{n_{states}} \end{bmatrix}
\end{aligned} \tag{24}$$

A standard second order system takes the following expression:

$$\begin{cases} \dot{\mathbf{x}}_1 = \mathbf{f}(\mathbf{x}_1) + \mathbf{g}\mathbf{x}_2 \\ \dot{\mathbf{x}}_2 = \mathbf{h}(\mathbf{x}_2) + \mathbf{k}\mathbf{u} \end{cases} \tag{25}$$

The backstepping procedure starts by defining the tracking errors as:

$$\mathbf{z}_1 = \mathbf{x}_1 - \mathbf{y}_r \mathbf{z}_2 = \mathbf{x}_2 - \alpha \tag{26}$$

where α is the virtual control to be designed in the first step.
Step 1: Rewriting the $\mathbf{z}_1$ dynamics

$$\dot{\mathbf{z}}_1 = \mathbf{f}(\mathbf{x}_1) + \mathbf{g}\mathbf{x}_2 - \dot{\mathbf{y}}_r = \mathbf{f}(\mathbf{x}_1) + \mathbf{g}(\alpha + \mathbf{z}_2) - \dot{\mathbf{y}}_r \tag{27}$$

We select Control Lyapunov Function (CLF):

$$V_1(\mathbf{z}_1) = \frac{1}{2}\left[\mathbf{z}_1^2 + \mathbf{k}_1\lambda_1^2\right] \tag{28}$$

where the gain $\mathbf{k}_1 > 0$ and the integrator term $\lambda_1 = \int_0^t \mathbf{z}_1 dt$ are introduced to eliminate the tracking error caused by the neglected control term. The derivative of V_1 is given by:

$$\dot{V}_1 = \mathbf{z}_1\dot{\mathbf{z}}_1 + \mathbf{k}_1\lambda_1\mathbf{z}_1 = \mathbf{z}_1\left[\mathbf{f}(\mathbf{x}_1) + \mathbf{g}\mathbf{x}_2 - \dot{\mathbf{y}}_r + \mathbf{k}_1\lambda_1\right] \tag{29}$$

The virtual control α is selected as:

$$\alpha = \mathbf{g}^{-1}\left[-\mathbf{c}_1\mathbf{z}_1 - \mathbf{f}(\mathbf{x}_1) + \dot{\mathbf{y}}_r - \mathbf{k}_1\lambda_1\right] \tag{30}$$

to render the derivative

$$\dot{V}_1 = -\mathbf{c}_1\mathbf{z}_1^2 \tag{31}$$

Step 2:
Rewriting the system in terms of the state $\mathbf{z}_1$ and $\mathbf{z}_2$:

$$\begin{cases} \dot{\mathbf{z}}_1 = \mathbf{f}(\mathbf{x}_1) + \mathbf{g}(\alpha + \mathbf{z}_2) - \dot{\mathbf{y}}_r \\ \dot{\mathbf{z}}_2 = \dot{\mathbf{x}}_2 - \dot{\alpha} = \mathbf{h}(\mathbf{x}_2) + \mathbf{k}\mathbf{u} - \dot{\alpha} \end{cases} \tag{32}$$

The CLF in Eq. 28 is augmented for the $(\mathbf{z}_1, \mathbf{z}_2)$-system with an extra term that penalizes the tracking error $\mathbf{z}_2$:

$$V_2(\mathbf{z}_1, \mathbf{z}_2) = \frac{1}{2}\mathbf{z}_1^2 + \frac{1}{2}\mathbf{k}_1\lambda_1^2 + \frac{1}{2}\mathbf{z}_2^2 + \frac{1}{2}\mathbf{k}_2\lambda_2^2 \tag{33}$$

with $\lambda_2 = \int_0^t \mathbf{z}_2 dt$. Taking the derivative of V_2 results in

$$\begin{aligned} \dot{V}_2 &= \mathbf{z}_1\dot{\mathbf{z}}_1 + \mathbf{k}_1\lambda_1\mathbf{z}_1 + \mathbf{z}_2\dot{\mathbf{z}}_2 + \mathbf{k}_2\lambda_2\mathbf{z}_2 \\ &= \mathbf{z}_1\left(\mathbf{f}(\mathbf{x}_1) + \mathbf{g}\left[\mathbf{g}^{-1}(-\mathbf{c}_1\mathbf{z}_1 - \mathbf{f}(\mathbf{x}_1) + \dot{\mathbf{y}}_r - \mathbf{k}_1\lambda_1) + \mathbf{z}_2\right] - \dot{\mathbf{y}}_r\right) \\ &+ \mathbf{k}_1\lambda_1\mathbf{z}_1 + \mathbf{z}_2(\mathbf{h}(\mathbf{x}_2) + \mathbf{k}\mathbf{u} - \dot{\alpha}) + \mathbf{k}_2\lambda_2\mathbf{z}_2 \\ &= -\mathbf{c}_1\mathbf{z}_1^2 + \mathbf{z}_2(\mathbf{g}\mathbf{z}_1 + \mathbf{h}(\mathbf{x}_2) + \mathbf{k}_2\lambda_2 + \mathbf{k}\mathbf{u} - \dot{\alpha}) \end{aligned} \tag{34}$$

Then we can get:

$$\mathbf{u} = \mathbf{k}^{-1}(-\mathbf{c}_2\mathbf{z}_2 - \mathbf{g}\mathbf{z}_1 + \dot{\alpha} - \mathbf{h}(\mathbf{x}_2) - \mathbf{k}_2\lambda_2) \tag{35}$$

In designing a sensor based backstepping (SBB) controller, we do not need to substitute $\dot{\mathbf{z}}_2 = \dot{\mathbf{x}}_2 - \dot{\alpha} = \mathbf{h}(\mathbf{x}_2) + \mathbf{k}\mathbf{u} - \dot{\alpha}$ in Eq. 34 and get:

$$\begin{aligned}\dot{V}_2 &= \mathbf{z}_1\dot{\mathbf{z}}_1 + \mathbf{k}_1\lambda_1\mathbf{z}_1 + \mathbf{z}_2\dot{\mathbf{z}}_2 + \mathbf{k}_2\lambda_2\mathbf{z}_2 \\ &= \mathbf{z}_1\left(\mathbf{f}(\mathbf{x}_1) + \mathbf{g}\left[\mathbf{g}^{-1}\left(-\mathbf{c}_1\mathbf{z}_1 - \mathbf{f}(\mathbf{x}_1) + \dot{\mathbf{y}}_r - \mathbf{k}_1\lambda_1\right) + \mathbf{z}_2\right] - \dot{\mathbf{y}}_r\right) \\ &+ k_1\lambda_1 z_1 + z_2\dot{z}_{2des} + k_2\lambda_2 z_2 \\ &= -\mathbf{c}_1\mathbf{z}_1^2 + \mathbf{z}_2\left(\mathbf{g}\mathbf{z}_1 + \mathbf{k}_2\lambda_2 + \dot{\mathbf{z}}_{2ref}\right)\end{aligned} \tag{36}$$

In order to make $\dot{V}_2$ negative definite, we can select:

$$\dot{\mathbf{z}}_{2ref} = -\mathbf{c}_2\mathbf{z}_2 - \mathbf{k}_2\lambda_2 - \mathbf{g}\mathbf{z}_1 \tag{37}$$

Hence, we can get:

$$\begin{aligned}\varepsilon\dot{\mathbf{u}} &= -sgn\left(\frac{\partial\dot{\mathbf{z}}_2}{\partial\mathbf{u}}\right)\cdot\left[\dot{\mathbf{z}}_2 - \dot{\mathbf{z}}_{2ref}\right] \\ \varepsilon\dot{\mathbf{u}} &= -sgn(\mathbf{k})\cdot\left[\dot{\mathbf{z}}_2 + \mathbf{g}\mathbf{z}_1 + \mathbf{k}_2\lambda_2 + \mathbf{c}_2\mathbf{z}_2\right]\end{aligned} \tag{38}$$

where $\dot{\mathbf{z}}_2 = \dot{\mathbf{x}}_2 - \dot{\alpha}$, $\dot{\mathbf{x}}_2$ is measurable and $\dot{\alpha}$ can be calculated according to Eq. 30. The configuration of the controller is depicted in the following framework:
where TA denotes the tuning algorithm (TA) block, *sgn and integration* denotes

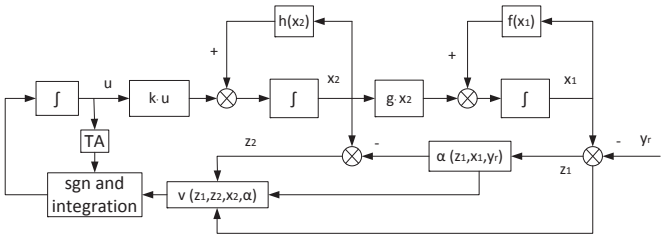

Fig. 2 Flow chart of the double-loop joint SBB attitude controller.

the block for executing the integration and sgn operation, and the following notation exists $v(\mathbf{z}_1,\mathbf{z}_2,\mathbf{x}_2,\alpha) := v(\dot{\mathbf{z}}_2,\mathbf{z}_1,\mathbf{z}_2) = [\dot{\mathbf{z}}_2 + \mathbf{g}\mathbf{z}_1 + \mathbf{c}_2\mathbf{z}_2]$. Note that, comparing with Eq. 17, the effects from the outer loop dynamics denoted by the term $\mathbf{g}\mathbf{z}_1$ are taken into account in the inner loop.

6 Results and Analysis

The proposed hybrid NDI/SSB attitude controller and joint SBB controller are evaluated using two fault scenarios named rudder runaway and right engine separation respectively. To obtain the simulation results in this section, the CA method shown in Eq. 8 and Eq. 9 is adopted.

6.1 Validation Results of the Nominal Aircraft using Joint SBB Controller

The command tracking results of the joint SBB attitude hold/change controller for nominal Boeing 747-aircraft, which uses the control setup shown in Fig. 1(b), are plotted in Figs.3(a)-3(h). Although we usually do not enforce a non-zero sideslip angle command in reality, we use a non-zero β command for the purpose of testing the control capacity of the developed controller. The idea of a fault-free test of the joint SBB controller is to show the pilot the capability of the proposed controller. The selected parameters of the controller are listed in Table 1. Fig. 3(a) shows the

Table 1 Joint controller parameters, nominal/engine separation

ε	$\mathbf{c}_1$	$\mathbf{k}_1$	$\mathbf{c}_2$	$\mathbf{k}_2$
0.4	$[1, 0.5, 0.65]$	$[0, 0, 0]$	$[1, 0.25, 0.5]$	$[0, 0, 0]$

direct inputs of the EPRs from the pilot. And the changing history of the total air velocity is plotted in Fig. 3(c). The the body angular rates are shown in Fig. 3(b), and they have zero values in steady level flight. The tracking performance of the attitude controller are depicted in Figs.3(d)-3(f). Step command inputs are added to pitch and roll angles at the 100^{th} and 200^{th} seconds separately, and the tracking errors equal to zero. Figs.3(g)-3(h) show the deflection of the control surfaces. In specific, Fig. 3(g) shows the deflecting values of the integrator output, and Fig. 3(h) shows the real deflection of each control surfaces subject to the physical limitations.

6.2 Validation of the Hybrid NDI/SBB Controller using Fault Scenarios

In the first simulation experiment, the hybrid NDI/SBB attitude hold controller using the propulsion control (PC) structure (see.Fig. 1(a)) is validated. The controller parameters are listed in Table 2. The validation results of the hybrid NDI/SBB at-

Table 2 Hybrid controller parameters, rudder runaway

ε	$\mathbf{P}_1$	$\mathbf{I}_1$	$\mathbf{c}_2$	$\mathbf{k}_2$
0.35	$[1, 1, 1]$	$[0.12, 0.12, 0.02]$	$[1, 1, 1]$	$[0.1, 0, 0]$

titude controller for the rudder runaway case are plotted in Figs.4(a)-4(h). Fig. 4(a) shows the control inputs of the EPRs, and all EPRs reach saturation limitation values after the rudder runaway failure occurs. The total air velocity, is controlled by the collective thrust, is illustrated in Fig. 4(c). As illustrated in Fig. 4(b), even the rudder runaway failure occurs, the body angular rates still keep around zeros.

The attitude control performance of the controller are revealed by Figs.4(d)-4(f). The failure is triggered at the 50^{th} second. At the 100^{th} and the 150^{th} seconds separately, a step command input is added to the pitch angle, and step inputs are added to the roll angle command at the 200^{th} and the 250^{th} seconds separately. The tracking errors of ϕ and θ equal to zero, while the tracking error of β stays around 2.8 degree. The non-zero tracking error of β may be caused by saturation of the EPR inputs. That is, zero β is not located in the reachable flight envelope under this failure. Figs.4(g)-4(h) show the changes of the control surface deflection. In specific, Fig. 4(g) shows the desired deflecting values, and Fig. 4(h) shows the real deflection of each control surfaces subject to the physical limitations. In the second simulation experiment, the hybrid attitude hold controller using the control structure shown in Fig. 1(b) is assessed. The controller parameters are listed in Table 3. The evaluation

Table 3 Parameters of the hybrid NDI/SBB controller, engine separation

ε	$\mathbf{P}_1$	$\mathbf{I}_1$	$\mathbf{c}_2$	$\mathbf{k}_2$
0.15	$[1,1,1]$	$[0.12,0.12,0.02]$	$[0.1,0.2,0.1]$	$[0.05,0,0]$

results of the hybrid NDI/SBB attitude controller under the right engine separation failure are plotted in Figs.5(a)-5(h). Fig. 5(a) shows the EPRs of the two remaining engines (Engine 1 and2). The total air velocity controlled by the collective thrust is illustrated in Fig. 5(c). As illustrated in Fig. 5(b), *p*,*q* and *r* still keep around zeros during steady level flight even though the rudder runaway failure occurs. The attitude control performance of the controller is depicted in Figs.5(d)-5(f). The tracking errors of ϕ and θ equal to zero, while the tracking error of β demonstrates oscillation around zero though it is under control. The non-zero tracking error of β may be caused by the physical (aerodynamic blow-down) limitation of the upper and lower rudders. That is, the remaining control capacity may be inadequate to compensate the yawing moment produced by the right engine separation. Fig. 5(g) and Fig. 5(h) show the deflecting angles of the control surfaces. In specific, Fig. 5(g) shows the desired deflecting values (i.e. the integrator output), and Fig. 5(h) shows the real deflecting angle of each control surfaces subject to the physical limitations. As illustrated in Fig. 5(h), neither the upper rudder nor the right outer aileron can contribute to the FTC operation, this is in consistent with the description of the rudder runaway scenario in Sec. 2.

6.3 Validation Results of the Joint SBB Attitude Controller

In the first simulation experiment, the joint SBB attitude hold controller using the structure shown in Fig. 1(a) is validated. The controller parameters are listed in Table 4. The validation results of the joint SBB attitude controller in the rudder runaway case are plotted in Figs.6(a)-6(h). All the results are similar to Figs.4(a)-4(h). Fig. 6(a) shows the control inputs of the EPRs, and all of the EPRs reach saturation

Table 4 Joint controller parameters, rudder runaway

ε	$\mathbf{c}_1$	$\mathbf{k}_1$	$\mathbf{c}_2$	$\mathbf{k}_2$
0.2	$[0.25, 0.2, 0.05]$	$[0.05, 0.05, 0.05]$	$[1, 1, 1]$	$[0, 0, 0]$

limitation values after the rudder runaway failure occurs. The attitude control performance of the joint SBB controller are depicted in Figs.6(d)-6(f). The tracking errors of ϕ and θ equal to zeros, while the tracking error of β stays around 2.5 degree. Comparing with the simulation results of the hybrid NDI/SBB controller for the same failure scenario (see.Figs.4(a)-4(h)), the control performance of the joint SBB controller is better than or equivalent to the former, especially when concerning β control.

In the second simulation experiment, the joint SBB attitude controller using the control structure shown in Fig. 1(b) is validated. The controller parameters are listed in Table 1. The evaluation results of the joint SBB attitude controller under the right engine separation failure are plotted in Figs.7(a)-7(h). Once again, these results are quite similar to those shown in Figs.5(a)-5(h). The attitude control performance of the joint SBB controller are depicted in Figs. 7(d)-7(f). The tracking errors of ϕ, θ and β equal to zeros. Figs.7(g)-7(h) show the deflection angles of the control surfaces. In specific, Fig. 7(g) shows the desired deflecting values (i.e. the integrator output), and Fig. 7(h) shows the real deflecting angle of each control surfaces subject to the physical limitations. As illustrated in Fig. 7(h), neither the upper rudder nor the right outer aileron has any contribution to the FTC operation due to their damages. Comparing with the simulation results using the hybrid NDI/SBB controller for the same failure scenario (see.Figs.5(a)-5(h)), the joint SBB controller has a better angular command control performance than the former, especially in terms of the sideslip angle and the roll angle control.

7 Conclusions

This paper has presented a joint SBB attitude flight control approach, which does not require the full model knowledge of the aircraft. The proposed SBB controllers are evaluated using two benchmark fault scenarios developed by the GARTEUR FM-AG 16. The simulation results show that the proposed SBB controllers can guarantee the stability of the aircraft even when the failures occur, and can make the close-loop system to track an attitude angle command with zero tracking error as long as the command is within the reachable flight envelope under the physical limitation of the available control surfaces. This paper has further extended the perturbation theory based incremental backstepping method proposed in [8] and the SBB method proposed in [4] to handle the multi-loop attitude tracking control and the FTFC problems associated with the failures. However, before real-life application, the proposed SBB method, especially for the rudder runaway scenario where a propulsion control (PS) structure is used, still need to be investigated about the

influence of the engine time-delay since the engine response has a significant lag, especially at low thrust levels.

References

1. Civil aviation safety data. Technical report, Civil Aviation Authority of the Netherlands, Netherlands (2003)
2. Alwi, H., Edwards, C., Stroosma, O., Mulder, J.A.: Evaluation of a sliding mode fault-tolerant flight controller for the el al incident. Journal of Guidance, Control and Dynamics **33**(3), 677–694 (2010)
3. Burcham, S., Kalmanje, K., Nhan, N.: Adaptive control of a transport aircraft using differential thrust. Nasa/tm-1998-206552, NASA Ames Research Center (1998)
4. Falkena, W., van Oort, E., Chu, Q.: Towards certifiable advanced flight control systems, a sensor based backstepping approach. In: AIAA Guidance, Navigation and Control Conference. AIAA, Portland, Oregon (2011)
5. Fuller, J.W.: Integrated flight propulsion control for loss-of-control prevention. In: AIAA Guidance, Navigation and Control Conference. AIAA, Minneapolis, Minnesota (2012)
6. Gilyard, G.B., Conley, J.L., Le, J., Burcham, J.F.W.: A simulation evaluation of a four–engine jet transport using engine trhust modulation for flightpath control. In: AIAA Guidance, Navigation and Control Conference. AIAA, Toronto, Ontario Canada (1991)
7. Halim, A.: Fault tolerant sliding mode control schemes with aerospace applications. Ph.D. thesis, University of Leicester, England (2008)
8. Hovakimyan, N., Lavretsky, E., Sasane, A.: Dynamic inversion for nonaffine-in-control systems via time-scale separation. Journal of Guidance, Control and Dynamics **13**(4), 451–465 (2007)
9. Lombaerts, T.J.: Fault tolerant flight control. Ph.D. thesis, Delft University of Technology, The Netherlands (2010)
10. Lombaerts, T.J., Smaili, M.H., Stroosma, O.: Piloted simulator evaluation results of new fault-tolerant flight control algorithm. Journal of Guidance, Control and Dynamics **32**(6), 1747–1765 (2009)
11. Pattern, R.: Fault tolerant control systems: The 1997 situation. In: Proceedings of IFAC Symposium on SAFEPROCESS. International Federation of Automatic Control, Laxenburg, Austria (1997)
12. Slotine, J.J.E., Li, W.: Applied Nonlinear Control. Prentice Hall, New Jersey (1991)
13. Smaili, M., Breeman, J., Lombaerts, T.: A simulation benchmark for aircraft survivability assessment. In: 26th International Congress of Aeronautical Sciences, pp. 1–12. The International Council of the Aeronautical Science, Anchorage, Alaska (2008)
14. Smaili, M., Breeman, J., Lombaerts, T., Joosten, D.: A simulation benchmark for integrated fault tolerant flight control evaluation. AIAA paper 2006-6471 (2006)
15. Smaili, M., Breeman, J., Lombaerts, T., Joosten, D.: A simulation benchmark for integrated fault tolerant flight control evaluation. Aiaa paper 2006-6471, AIAA (2006)
16. Vahram, S., Kalmanje, K., Nhan, N.: Adaptive control of a transport aircraft using differential thrust. Nasa technical paper 1108, NASA Ames Research Center, Moffett Field (2009)
17. Zhang, Y.: Fault tolerant control systems:historical review and current research. technical paper, Centre de Recherche en Automatique de Nancy, Nancy, France (2005)
18. Zhang, Y., Jiang, J.: Bibliographical review on reconfigurable fault-tolerant control systems. In: 5th IFAC Symposium on Fault Detection, Supervision and Safety for Technical Processes. International Federation of Automatic Control, Laxenburg, Austria (2003)

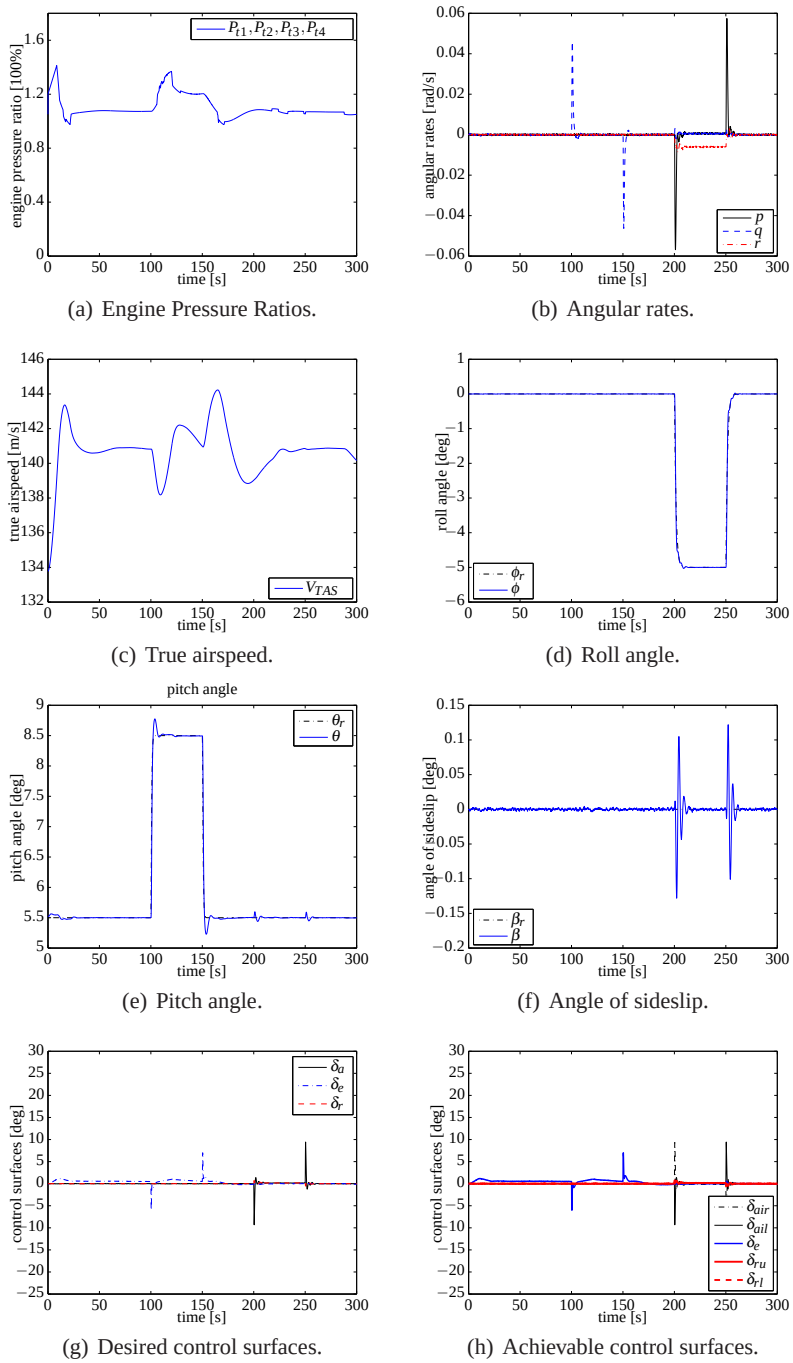

(a) Engine Pressure Ratios. (b) Angular rates.

(c) True airspeed. (d) Roll angle.

(e) Pitch angle. (f) Angle of sideslip.

(g) Desired control surfaces. (h) Achievable control surfaces.

Fig. 3 Simulation results of the joint controller for nominal aircraft.

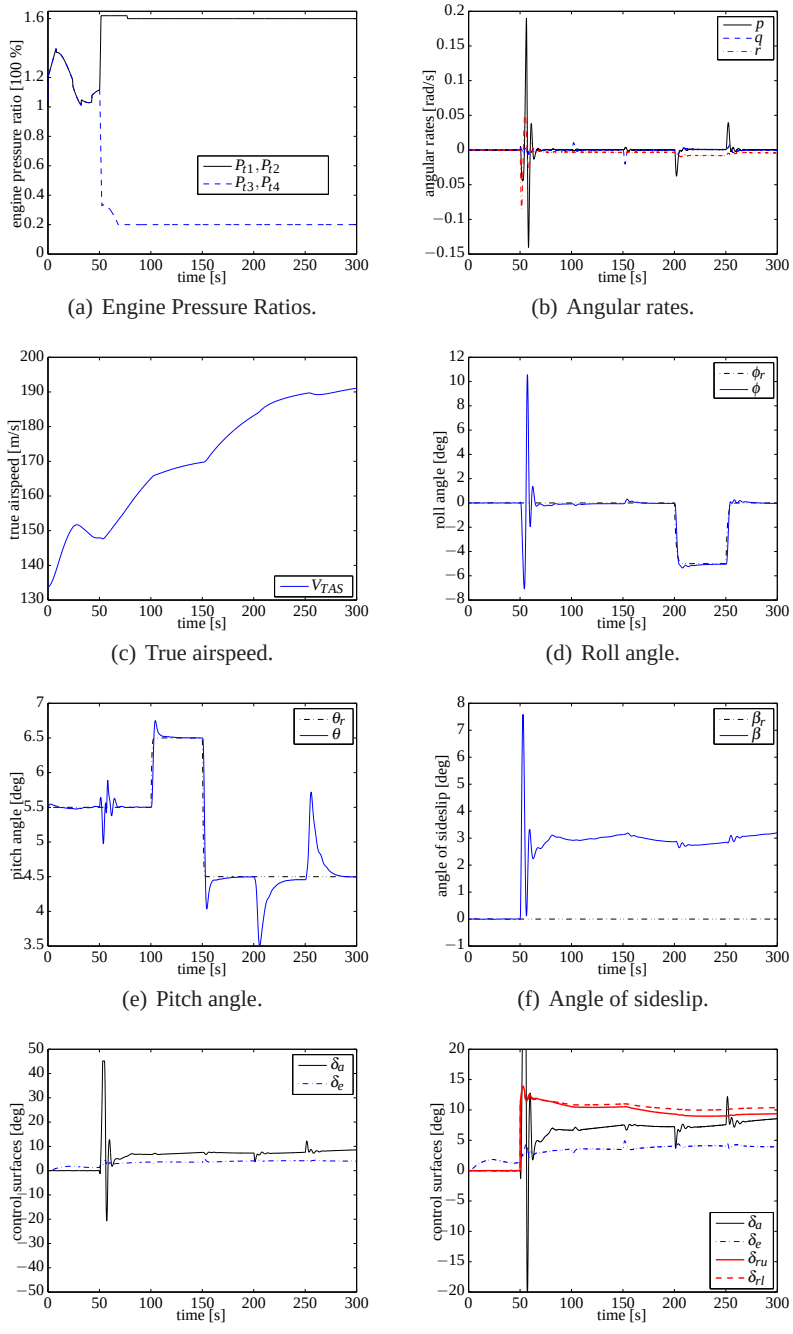

(a) Engine Pressure Ratios. (b) Angular rates.

(c) True airspeed. (d) Roll angle.

(e) Pitch angle. (f) Angle of sideslip.

(g) Desired control surfaces. (h) Achievable control surfaces.

Fig. 4 Simulation results of the hybrid controller for the rudder runaway case.

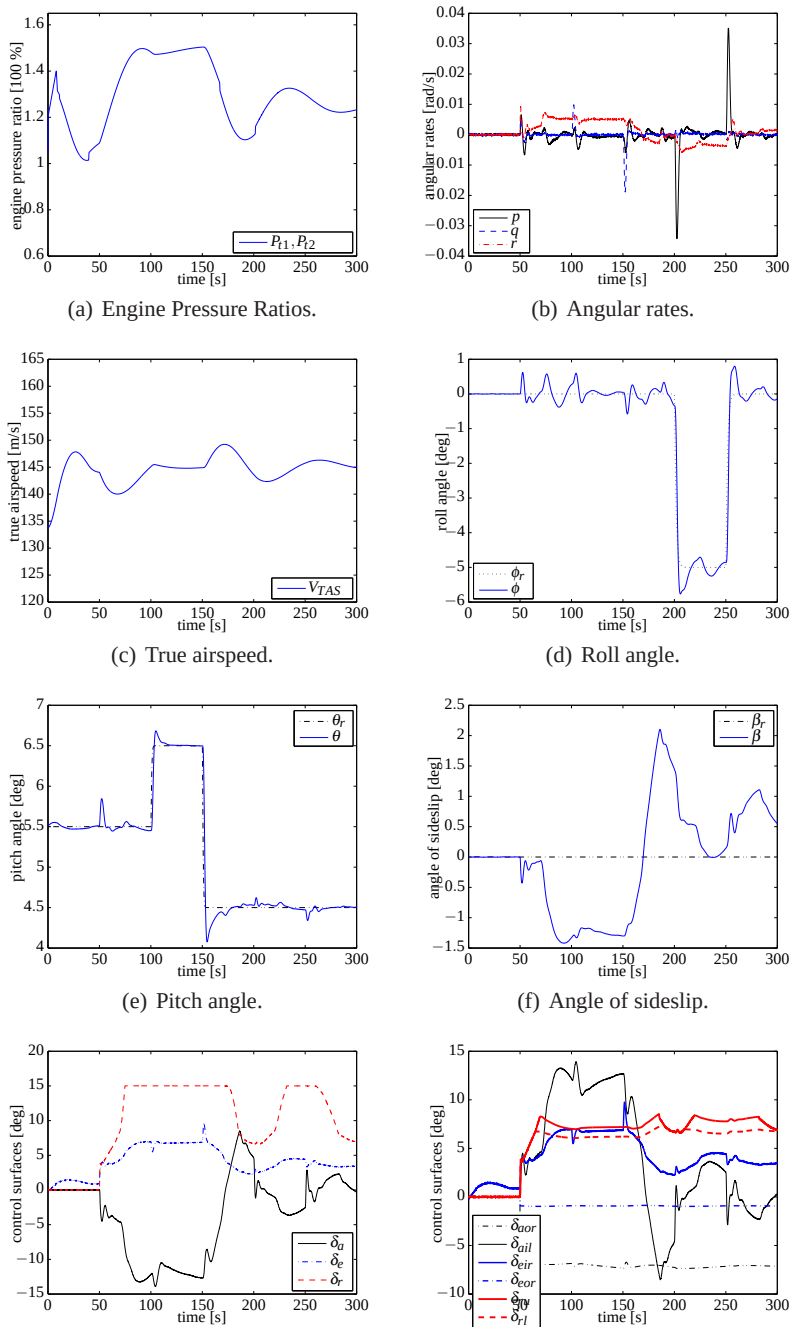

(a) Engine Pressure Ratios. (b) Angular rates.

(c) True airspeed. (d) Roll angle.

(e) Pitch angle. (f) Angle of sideslip.

(g) Desired control surfaces. (h) Achievable control surfaces.

Fig. 5 Simulation results of the hybrid controller for the engine separation case.

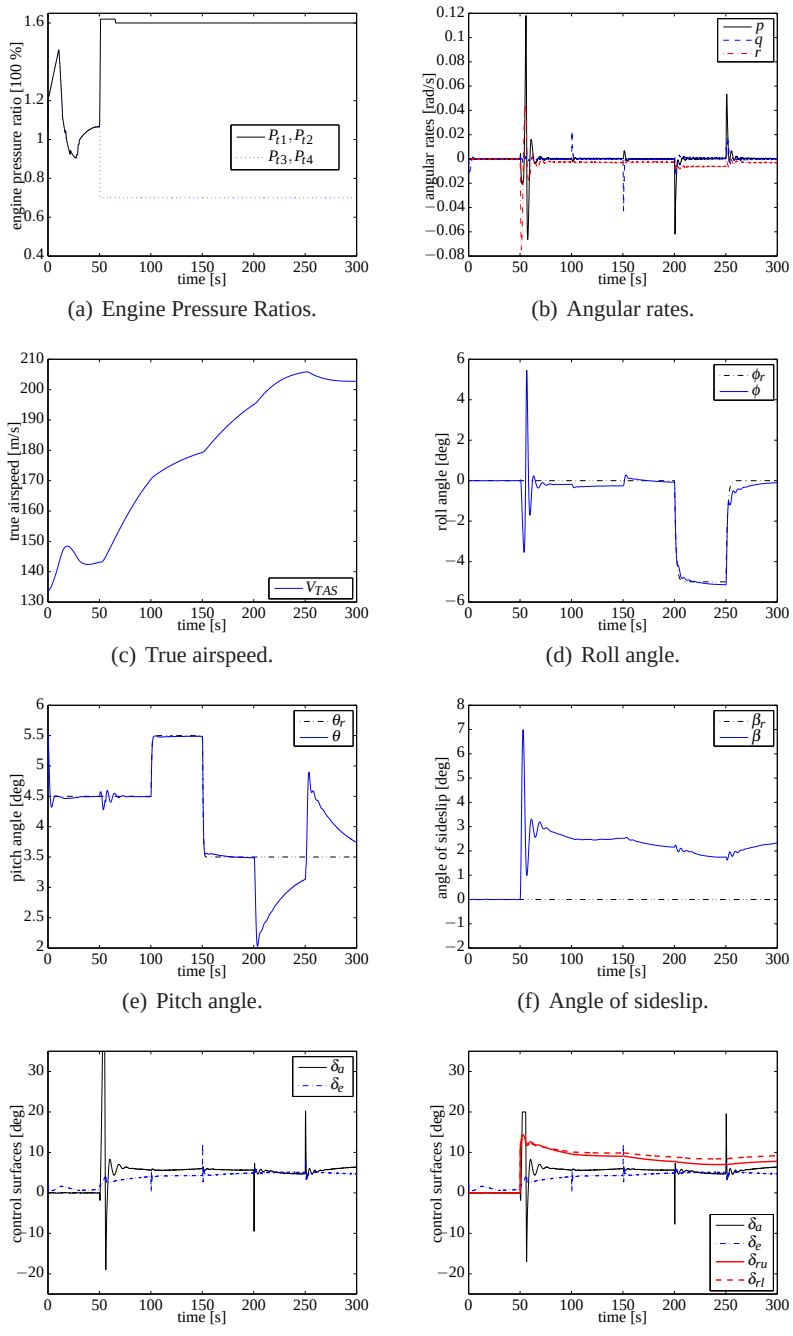

(a) Engine Pressure Ratios. (b) Angular rates.

(c) True airspeed. (d) Roll angle.

(e) Pitch angle. (f) Angle of sideslip.

(g) Desired control surfaces. (h) Achievable control surfaces.

Fig. 6 Simulation results of the joint controller for the rudder runaway case.

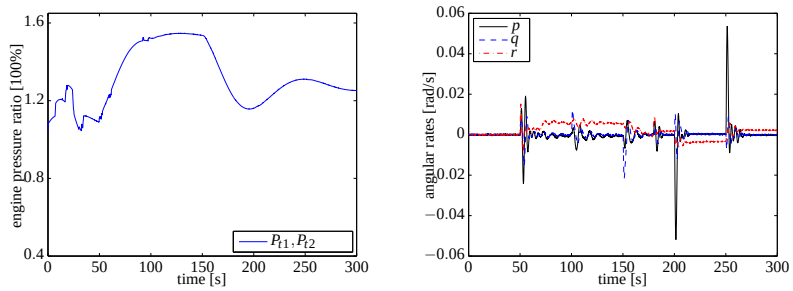

(a) Engine Pressure Ratios.

(b) Angular rates.

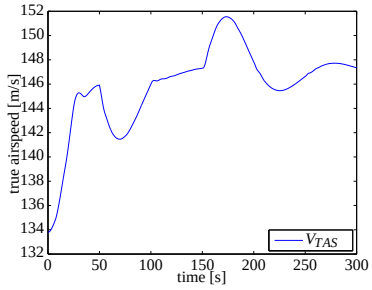

(c) True airspeed.

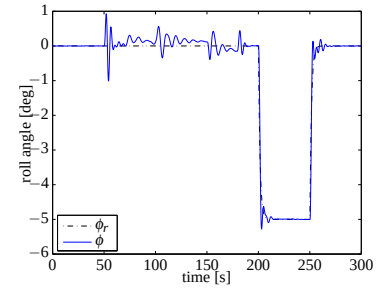

(d) Roll angle.

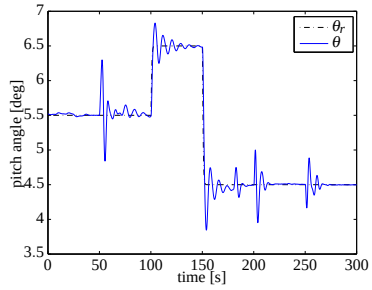

(e) Pitch angle.

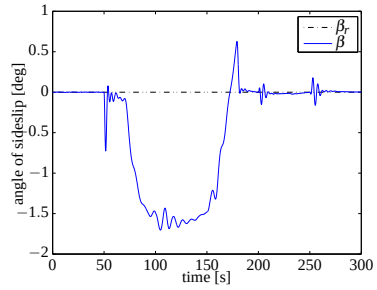

(f) Angle of sideslip.

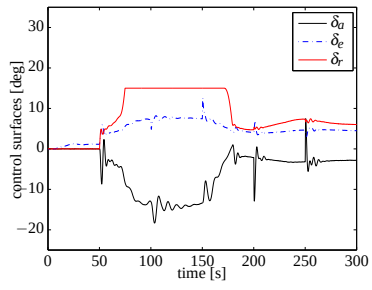

(g) Desired control surfaces.

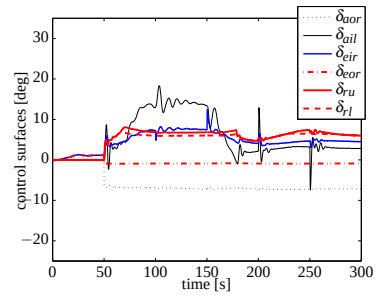

(h) Achievable control surfaces.

Fig. 7 Simulation results of the joint controller for the engine separation case.